Biogeosciences
Discussions

Open Access

Technical Note: Simple formulations and solutions of the dual-phase diffusive transport for biogeochemical modeling

J. Y. Tang and W. J. Riley

Department of Climate and Carbon Sciences, Earth Sciences Division, Lawrence Berkeley National Lab (LBL), Berkeley, CA, USA

Correspondence to: J. Y. Tang (jinyuntang@lbl.gov)

Full Screen / Esc

Printer-friendly Version

Interactive Discussion

Abstract

Representation of gaseous diffusion in variably saturated near-surface soils is becoming more common in land biogeochemical models, yet the formulations and numerical solution algorithms applied vary widely. We present three different but equivalent formulations of the dual-phase (gaseous and aqueous) tracer diffusion transport problem that is relevant to a wide class of volatile tracers in land biogeochemical models. Of these three formulations (i.e., the gas-primary, aqueous-primary, and bulk tracer based formulations), we contend the gas-primary formulation is the most convenient for modeling tracer dynamics in biogeochemical models. We then provide finite volume approximation to the gas-primary equation and evaluate its accuracy against three analytical models: one for steady-state soil CO_2 dynamics, one for steady-state soil CO_2 dynamics, and one for transient tracer diffusion from a constant point source into two different sequentially aligned medias. All evaluations demonstrated good accuracy of the numerical approximation. We expect our result will standardize an efficient mechanistic numerical method for solving relatively simple, multi-phase, one-dimensional diffusion problems in land models.

1 Introduction

The interest in predicting fluxes of various biogenic greenhouse gases and their interactions with climate change has motivated the development of many terrestrial biogeochemical models; e.g., ecosystem methane models (Walter and Heiman, 2000; Zhuang et al., 2004; Tang et al., 2010; Riley et al., 2011), nitrification-denitrification models (Venterea and Rolston, 2000; Maggi et al., 2008), water-CO_2 isotope models (Riley et al., 2002), and generic reactive transport models that attempt to integrate as many biogeochemical processes and chemical species as possible (e.g., Simunek and Suarez, 1993; Grant, 2001; Tang et al., 2013). To resolve the depth-dependent dy-

namics, these models in general represent multiphase (aqueous and gaseous phase) diffusion processes and often assume negligible advection.

The equation for multiphase diffusion has been represented in different forms by different authors (Table 1). However, the numerical implementation of the equation is often vaguely described (either by referring to other publications or by mentioning the numerical scheme) or is convolved with other technical details, making the model difficult to understand or replicate by other researchers. In many cases, however, one does not need to represent all the processes typically included in a complicated reactive transport model to understand a particular problem. For instance, when soil moisture and temperature data are available together with soil respiration, one only needs a diffusion model to evaluate belowground CO_2 dynamics (Davidson et al., 2006). Therefore, ecosystem models would benefit from a simple mechanistic formulation and numerical implementation of the dual-phase diffusion problem.

In this note, we categorize the existing formulations of the dual-phase diffusion problem into three forms, and recommend one that can be most easily implemented numerically in land models. We hope that this effort will help researchers who wish to develop simple but mechanistic transport models for their particular problem.

2 Methods

2.1 Governing equations

In this section we derive the relevant mass balance differential equations from first principles. Throughout this note we assume advection is treated using the operator splitting method (Tang et al., 2013), or is negligible. Considering the diffusive mass transport problem (Fig. 1), the dual-phase diffusive flux from layer $j-1$ into j is

$$F_{j-1\to j} = F_{w,j-1\to j} + F_{g,j-1\to j} \tag{1a}$$

$$F_{w,j-1 \to j} = -\left(\theta D_w \frac{\partial C_w}{\partial z} \right)_{j-\frac{1}{2}} \tag{1b}$$

$$F_{g,j-1 \to j} = -\left(\varepsilon D_g \frac{\partial C_g}{\partial z} \right)_{j-\frac{1}{2}} \tag{1c}$$

where subscript w indicates aqueous diffusion and subscript g indicates gaseous diffusion. Soil moisture is represented by θ and air-filled porosity by ε. The fluxes ($F_{j-1 \to j}$) are imposed at the upper and lower boundaries of layer j. Tracer concentrations are designated by C with appropriate subscripts. In defining the effective aqueous (D_w) and gaseous (D_g) diffusivities, we assume the tortuosity has been considered appropriately (e.g., Moldrup et al., 2003). A full list of symbols is given in Table A1.

Applying the law of mass balance to layer j

$$\Delta z_j \frac{\Delta C_j}{\Delta t} = F_{j-1 \to j} - F_{j \to j+1} = \left(F_{w,j-1 \to j} - F_{w,j \to j+1} \right) + \left(F_{g,j-1 \to j} - F_{g,j \to j+1} \right) + S_j \Delta z_j \tag{2a}$$

and in the limit of small Δz_j and Δt, one obtains

$$\frac{\partial C}{\partial t} = \frac{\partial}{\partial z} \left(\theta D_w \frac{\partial C_w}{\partial z} \right) + \frac{\partial}{\partial z} \left(\varepsilon D_g \frac{\partial C_g}{\partial z} \right) + S(C,z) \tag{2b}$$

where $S(C,z)$ is the tracer source due to processes other than diffusion and C is the bulk tracer concentration including both gaseous and aqueous phases. From the assumption of equilibrium between aqueous and gaseous phases (e.g., Tang et al., 2010):

$$C = \theta C_w + \varepsilon C_g = R_g C_g = (\theta \alpha + \varepsilon) C_g = R_w C_w = \left(\theta + \frac{\varepsilon}{\alpha} \right) C_w \tag{3}$$

1590

where α is the Bunsen solubility coefficient, one obtains, from substitution of Eq. (3) into the diffusion and temporal derivative of Eq. (2b):

$$R_g \frac{\partial C_g}{\partial t} = \frac{\partial}{\partial z}\left[(\alpha\theta D_w + \varepsilon D_g)\frac{\partial C_g}{\partial z}\right] + S(C,z) \tag{4a}$$

$$R_w \frac{\partial C_w}{\partial t} = \frac{\partial}{\partial z}\left[\left(\theta D_w + \frac{\varepsilon}{\alpha}D_g\right)\frac{\partial C_w}{\partial z}\right] + S(C,z) \tag{4b}$$

By further defining a bulk diffusivity

$$D = \frac{\alpha\theta D_w + \varepsilon D_g}{R_g} = \frac{\theta D_w + \varepsilon D_g/\alpha}{R_w} \tag{5}$$

and assuming

$$\left|\frac{1}{C_x}\frac{\partial C_x}{\partial t}\right| \gg \left|\frac{1}{R_x}\frac{\partial R_x}{\partial t}\right|, \left|\frac{1}{C_x}\frac{\partial C_x}{\partial z}\right| \gg \left|\frac{1}{R_x}\frac{\partial R_x}{\partial z}\right|, \ x = \text{w or g} \tag{6}$$

one finds for the bulk tracer:

$$\frac{\partial C}{\partial t} = \frac{\partial}{\partial z}\left(D\frac{\partial C}{\partial z}\right) + S(C,z) \tag{7}$$

Clearly, Eqs. (4a) (gas-primary form), (4b) (aqueous-primary form), and (7) (bulk tracer form) are equivalent, but Eq. (4) are more convenient to solve because the tracer sources are in general given as aqueous reactions or gaseous sinks (e.g., plant transport, ebullition) and the necessary phase conversion can be done easily through Eq. (3). In particular, Eq. (4a) (the gas-primary form) is the most convenient for simulating volatile tracers and can be applied to variably saturated soil without the need for special care of the air–water interface, as was done in a few existing wetland-CH_4 models (see remark in Table 1). We note that Eq. (4a) was also used by Simunek and Suarez (1993) to model CO_2 transport in soil.

At the top boundary, conditions are in general given as gas tracer concentrations, which are connected to the gas concentration of the top numerical layer as

$$F_{g,0 \to 1} = -\frac{C_{g,1} - C_a}{r_a + r_s} \tag{8}$$

where r_a is atmospheric resistance and r_s is soil resistance (see Tang and Riley, 2013, for a detailed discussion).

At the bottom boundary, zero flux conditions are often imposed, though zero concentration can also be used for particular problems. In practice, if a tracer exists only in the aqueous phase, then one can solve Eq. (4b) for aqueous diffusive transport by setting $\alpha \to \infty$ and using a zero-flux boundary condition at the top and bottom boundaries.

2.2 Numerical implementation

We now solve Eq. (4a) using the finite volume method. First, we discretize the equation spatially and convert it into the following ordinary differential equation (ODE) system,

$$\text{diag}\left(Z_g\right) \frac{\mathrm{d}C_g}{\mathrm{d}t} = \mathbf{A}C_g + S \tag{9a}$$

where $\text{diag}(V)$ indicates a diagonal matrix formed by the vector V and

$$C = \begin{bmatrix} C_{g,1} \cdots C_{g,j} \cdots C_{g,N} \end{bmatrix}^T \tag{9b}$$

$$\mathbf{A} = \begin{bmatrix} -c_{1/2} - c_{3/2} & c_{3/2} & 0 & \cdots & 0 \\ \vdots & \vdots & \vdots & \cdots & 0 \\ \cdots & c_{j-1/2} & -c_{j-1/2} - c_{j+1/2} & c_{j+1/2} & \cdots \\ \vdots & 0 & \cdots & \cdots & \vdots \\ 0 & \cdots & 0 & c_{N-1/2} & -c_{N-1/2} - c_{N+1/2} \end{bmatrix} \tag{9c}$$

$$S = \begin{bmatrix} S\left(C_1, z_1\right) \Delta z_1 + c_{1/2} C_a \cdots S\left(C_j, z_j\right) \Delta z_j \cdots S\left(C_N, z_N\right) \Delta z_N + c_{N+1/2} C_b \end{bmatrix}^T \tag{9d}$$

$$Z_g = \left[R_{g,1} \Delta z_1 \cdots R_{g,j} \Delta z_j \cdots R_{g,N} \Delta z_N \right] \qquad (9e)$$

Other coefficients are defined as

$$D_{wg,j} = \alpha_j \theta_j D_{w,j} + \varepsilon_j D_{g,j}, \quad 1 < j \leq N \qquad (10a)$$

$$c_{j-1/2} = \left(\frac{\Delta z_{j-1}}{2D_{wg,j-1}} + \frac{\Delta z_j}{2D_{wg,j}} \right)^{-1}, \quad 1 < j \leq N \qquad (10b)$$

$$c_{1/2} = \frac{1}{r_a + r_s} \qquad (10c)$$

Conductance $c_{N+1/2}$ is zero when zero flux bottom boundary condition is used, but here it is included to enable Eq. (9) to accommodate the bottom boundary condition given as a constant tracer concentration (C_b). For this latter case, one can simply set $c_{N+1/2}$ to $c_{N-1/2}$.

The ODE system formed by Eq. (9) (together with Eq. 10) can be easily solved with various temporal discretization methods. For instance, the ODE solvers (e.g., ODE45, ODE23) in MATLAB provide a very straightforward way to obtain the solutions. In addition, we point out that by solving the equation implicitly with a very large time step (as we have done for our evaluation against steady-state analytical results below), Eq. (9) can also provide the steady state solution that has been used in several models to derive rates of soil methane consumption and production (Curry, 2007; Zhuang et al., 2004, 2013). However, our formulation is more general and can be applied to model multiple gas species simultaneously.

The aqueous-primary equation Eq. (4b) can be solved analogously, but it should be processed with appropriate definitions of the conductances.

2.3 Evaluation with analytic models

We used two steady state analytic models and one transient analytical model to evaluate the spatial discretization in Eqs. (9) and (10).

The first analytical model is the steady state CO_2 diffusion model presented in Tans (1998), but we added aqueous diffusion, which was not included in his Eq. (2). The governing equation of the modified Tans model is

$$\left(\varepsilon D_g + \theta D_w\right) \frac{d^2 C_g}{dz^2} + S_o \exp\left(-\frac{z}{z_0}\right) = 0 \tag{11}$$

whose solution is

$$C_g(z) = \frac{S_o}{\varepsilon D_g + \theta D_w} z_0^2 \left[1 - \exp\left(-\frac{z}{z_0}\right)\right] + C_a \tag{12}$$

We list the parameter values used in our example application in Table 2.

We craft the second model to mimic the methane cycle in a peatland, with methane consumption in the unsaturated topsoil (defined as from the soil surface to depth z_1, below which the soil is saturated) and a constant methane production from depth z_1 to z_2. We could have replicated published methane models and compared with pore-water CH_4 concentrations, but other uncertainties (e.g., uncertainties in parameterization, formulation, and measurement) would obfuscate a direct evaluation of the accuracy of our diffusive transport numerical formulation.

The governing equation of the steady-state methane model is

$$\left(\varepsilon_1 D_g + \alpha \theta_1 D_w\right) \frac{d^2 C_g}{dz^2} - Q_1 \theta_1 C_w = 0, \text{ for } 0 \leq z \leq z_1 \tag{13a}$$

$$(\alpha \theta_2 D_w) \frac{d^2 C_g}{\partial z^2} + Q_2 = 0, \text{ for } z_1 < z < z_2 \tag{13b}$$

$$\left[\left(\varepsilon_1 D_g + \alpha \theta_1 D_w\right) \frac{dC_g}{dz}\right]_{z_1^-} = \left(\alpha \theta_s D_w \frac{dC_g}{dz}\right)_{z_1^+} \tag{13c}$$

$$\frac{dC_g}{dz} = 0, \text{ for } z \geq z_2 \tag{13d}$$

whose solution is found (see Supplement) as

$$C_g(z) = \frac{C_a \exp\left(\sqrt{\frac{\alpha\theta_1 Q_1}{D_1}}z_1\right) - \frac{Q_2}{D_1}\sqrt{\frac{D_1}{\alpha\theta_1 Q_1}}(z_2 - z_1)}{\exp\left(-\sqrt{\frac{\alpha\theta_1 Q_1}{D_1}}z_1\right) + \exp\left(\sqrt{\frac{\alpha\theta_1 Q_1}{D_1}}z_1\right)} \exp\left(-\sqrt{\frac{\alpha\theta_1 Q_1}{D_1}}z\right) \tag{14a}$$

$$+ \frac{C_a \exp\left(-\sqrt{\frac{\alpha\theta_1 Q_1}{D_1}}z_1\right) + \frac{Q_2}{D_1}\sqrt{\frac{D_1}{\alpha\theta_1 Q_1}}(z_2 - z_1)}{\exp\left(-\sqrt{\frac{\alpha\theta_1 Q_1}{D_1}}z_1\right) + \exp\left(\sqrt{\frac{\alpha\theta_1 Q_1}{D_1}}z_1\right)} \exp\left(\sqrt{\frac{\alpha\theta_1 Q_1}{D_1}}z\right), \text{ for } 0 \leq z \leq z_1$$

$$C_g(z) = \frac{Q_2}{D_2}(z - z_1)(z_2 - z_1) - \frac{Q_2}{2D_2}(z - z_1)^2 + C_g(z_1), \text{ for } z_1 < z < z_2 \tag{14b}$$

$$C_g(z) = \frac{Q_2}{2D_2}(z_2 - z_1)^2 + C_g(z_1), \text{ for } z \geq z_2 \tag{14c}$$

where $D_1 = \varepsilon_1 D_g + \alpha\theta_1 D_w$ and $D_2 = \alpha\theta_2 D_w$. Parameter values used in our example application are listed in Table 3.

The transient model considers the release of a tracer from a constant point source (C_0) into a media, which is connected to another media at some distance z_1. The tracer has different diffusivities and solubilities in the two media, and its concentration is kept zero at the bottom of the second media. The model solves for the temporal evolution of the tracer in both media. Mathematically, the model is formulated as

$$\frac{\partial C_g}{\partial t} = D_g \frac{\partial^2 C_g}{\partial z^2}, \text{ for } 0 < z < z_1 \tag{15a}$$

$$\frac{\partial C_g}{\partial t} = D_w \frac{\partial^2 C_g}{\partial z^2}, \text{ for } z_1 < z < L \tag{15b}$$

$$\left(D_g \frac{\partial C_g}{\partial z}\right)_{z_1^-} = \left(D_w \alpha \frac{\partial C_g}{\partial z}\right)_{z_1^+} \tag{15c}$$

$$C_g\left(z_1^+\right) = C_g\left(z_1^-\right) \tag{15d}$$

where we note the variables in Eq. (15) are now not necessarily related to gaseous and aqueous phases, but we simply keep the denotations for simplicity. The initial condition to Eq. (15) is set as zero tracer concentration everywhere inside the column.

The model represented by Eq. (15) can represent a few different problems, such as contaminant diffusion from human skin into blood (e.g., Riley et al., 2004) or heat conduction between two metals of an alloy (e.g., Carslaw and Jaeger, 1986). When all coefficients are given as constant, Eq. (15) has the analytic solution (Carslaw and Jaeger, 1986):

$$
\begin{aligned}
C_g\left(z \le z_1\right) = &\frac{C_0\left(D_g L/\alpha - D_w s\right)}{D_g L/\alpha + D_w z_1} \\
&- 2C_0 \sum_{n=1}^{\infty} \frac{\sin^2\left(kL\beta_n\right)\sin\left(\beta_n z\right)}{\beta_n\left[z_1 \sin^2\left(kL\beta_n\right) + \alpha L \sin^2\left(z_1\beta_n\right)\right]} \exp\left(-D_g \beta_n^2 t\right)
\end{aligned}
\tag{16a}
$$

$$
\begin{aligned}
C_g\left(z \ge z_1\right) = &\frac{D_g C_0\left(L - s\right)}{D_g L + D_w z_1 \alpha} \\
&- 2C_0 \sum_{n=1}^{\infty} \frac{\sin\left(z_1\beta_n\right)\sin\left(kL\beta_n\right)\sin\left(k\left(L-s\right)\beta_n\right)}{\beta_n\left[z_1 \sin^2\left(kL\beta_n\right) + \alpha L \sin^2\left(z_1\beta_n\right)\right]} \exp\left(-D_g \beta_n^2 t\right)
\end{aligned}
\tag{16b}
$$

where $s = z - z_1$, $k = \sqrt{D_g/D_w}$. The eigenvalues, β_n, are solutions of

$$\cos\left(\beta z_1\right)\sin\left(k\beta L\right) + \sigma \sin\left(\beta z_1\right)\cos\left(k\beta L\right) = 0 \tag{16c}$$

which is solved by Newton iteration methods. In evaluating Eq. (16), we only used the first 17 eigenvalues, because more eigenvalues did not significantly improve the estimation. Parameter values for the example application are listed in Table 4.

In all numerical experiments, we discretized the vertical soil profile using a scheme modified from CLM4.5 (Oleson et al., 2013), which defines the node depth of layer j as

$$z_j = \begin{cases} f_{s,1} \left\{ \exp \left[f_{s,2} (j - 0.5) \right] - 1 \right\}, & j = 1, \cdots, N-1 \\ (2L + z_{N-1})/3 \, j = N \end{cases}$$ (17a)

and the thickness of each layer as

$$\Delta z_j = \begin{cases} 0.5 (z_1 + z_2) & j = 1 \\ 0.5 (z_{j+1} - z_{j-1}) & j = 2, 3, \cdots, N-1 \\ 2 (L - z_{N-1})/3 & j = N \end{cases}$$ (17b)

and the depth at interfaces as

$$z_{h,j} = \begin{cases} 0.5 (z_j + z_{j+1}) & j = 1, 2, \cdots, N-1 \\ z_N + 0.5 \Delta z_N & j = N \end{cases}$$ (17c)

For all numerical experiments, the total soil column depth is set to 3.7 m. For the numerical approximation to the transient problem, the Crank–Nicholson method (Crank and Nicholson, 1947) is used for temporal discretization.

3   Results and discussion

Driven by the prescribed CO_2 source (Fig. 2a), the numerical solution using 100 numerical layers predicts a soil CO_2 profile very close to the exact solution throughout the soil column (Fig. 2b). The maximum relative error is about 0.2 %, which is hard to discern

visually. Decreasing the number of numerical layers to 20 leads to visually discernible deviations from the analytic solution and the maximum relative error increases to ∼ 4 %. However, the maximum relative error in both cases is near the surface, where the CO_2 concentration is low. The 20- and 100-layer simulations predict a surface CO_2 efflux of about 1 % and 0.03 % accuracy, respectively, with respect to the analytical flux. These results indicate our numerical technique is sufficient for most soil dual-phase diffusion modeling applications.

The evaluation of the CH_4 numerical solution against the analytical CH_4 model in general shows good accuracy. As for CO_2, more numerical layers lead to better numerical accuracy. Both 20-layer and 100-layer solutions indicate significant deviations from the analytical soil CH_4 profile, but the largest relative error is about 5 % for the 20-layer simulation and less than 1 % for the 100-layer simulation. The largest relative error occurs at the bottom of the topsoil (10 cm) in both cases. Because of the numerical approximation, both numerical solutions do not have numerical layers interfaced at 10 cm, which, when combined with the abrupt transition from the first order consumption in topsoil to the constant methane production rate between 10 cm and 40 cm, lead to the largest relative error. Nevertheless, considering that the 20-layer and 100-layer solutions have 7 % and 3 % relative error, respectively, in approximating the surface methane fluxes, the numerical algorithm should again satisfy the needs of modeling methane dynamics in ecosystem biogeochemical models.

For the transient model, we first compared the temporal evolution of tracer concentrations at three depths (7 cm, 15 cm, and 200 cm) (Fig. 4a–c, respectively). Again, both the 20-layer and 100-layer simulations show visually very accurate results (with mean relative error less than 5 % for the 20-layer and less than 1 % for the 100-layer) though there are large errors (> 100 %) in the first ten minutes of the simulations (when tracer concentrations are very low), which are probably caused by errors in both the finite volume approximation and the numerical error in evaluating the analytic results (see Fig. S1 for the latter case). When the steady state solutions are compared (Fig. 4d), the two numerical models show mean relative error within 2 %, indicating our numerical

J. Y. Tang and W. J. Riley

algorithm are very accurate. In both transient and steady state cases, the numerically predicted top surface fluxes agree with the analytical solution with a mean relative error within 10 % for the 20-layer and 2 % for the 100-layer simulations, respectively, after the first twenty minutes of simulation.

To summarize from the three evaluations, we contend Eq. (4a) and its approximation Eq. (9) should be very helpful for solving the dual-phase diffusion problem.

4   Conclusion

Dual-phase diffusion is an important process that needs to be represented in depth-resolved biogeochemical models. Here we reviewed existing formulations in the literature and categorized three forms used in biogeochemical models. We recommend that the gas-primary form (Eq. 4a) is the most convenient to solve. Its finite volume approximation can represent tracer transport in variably saturated soils without the need for special treatment of the air–water interface (as is often done in existing methane models). Our evaluation of the numerical algorithm with three analytical models demonstrated good accuracy of our numerical model, with some dependence on spatial discretization. We hope our results can help researchers develop simple but mechanistic models for some scientific questions where more complex reactive-transport models are not necessary.

Supplementary material related to this article is available online at http://www.biogeosciences-discuss.net/11/1587/2014/ bgd-11-1587-2014-supplement.pdf.

References

Carslaw, H. S. and Jaeger, J. C.: Conduction of Heat in Solids, 2nd edn., Clarendon Press, Oxford University Press, Oxford Oxfordshire, New York, viii, 510 pp., 1986.

Crank, J. and Nicolson, P.: A practical method for numerical evaluation of solutions of partial differential equations of the heat-conduction type, P. Camb. Philos. Soc., 43, 50–67, 1947.

Curry, C. L.: Modeling the soil consumption of atmospheric methane at the global scale, Global Biogeochem. Cy., 21, Gb4012, doi:10.1029/2006gb002818, 2007.

Davidson, E. A., Savage, K. E., Trumbore, S. E., and Borken, W.: Vertical partitioning of CO_2 production within a temperate forest soil, Glob. Change Biol., 12, 944–956, doi:10.1111/J.1365-2486.2005.01142.X, 2006.

Grant, R. F.: A review of the Canadian ecosystem model ecosys, in: Modeling Carbon and Nitrogen Dynamics for Soil Management, CRC Press, Boca, Raton, 173–264, ISBN 10: 1566705290, 2001.

Maggi, F., Gu, C., Riley, W. J., Hornberger, G. M., Venterea, R. T., Xu, T., Spycher, N., Steefel, C., Miller, N. L., and Oldenburg, C. M.: A mechanistic treatment of the dominant soil nitrogen cycling processes: model development, testing, and application, J. Geophys. Res.-Biogeo., 113, G02016, doi:10.1029/2007jg000578, 2008.

Moldrup, P., Olesen, T., Komatsu, T., Yoshikawa, S., Schjonning, P., and Rolston, D. E.: Modeling diffusion and reaction in soils: X. A unifying model for solute and gas diffusivity in unsaturated soil, Soil Sci., 168, 321–337, doi:10.1097/00010694-200305000-00002, 2003.

Oleson, K., Lawrence, D. M., Bonan, G. B., Drewniak, B., Huang, M., Koven, C. D., Levis, S., Li, F., Riley, W. J., Subin, Z. M., Swenson, S., Thornton, P. E., Bozbiyik, A., Fisher, R., Heald, C. L., Kluzek, E., Lamarque, J.-F., Lawrence, P. J., Leung, L. R., Lipscomb, W., Muszala, S. P., Ricciuto, D. M., Sacks, W. J., Sun, Y., Tang, J., and Yang, Z.-L.: Technical description of version 4.5 of the Community Land Model (CLM), NCAR Technical Note NCAR/TN-503+STR, 420 pp., doi:10.5065/D6RR1W7M, 2013.

Simple formulations and solutions of the dual-phase diffusive transport

J. Y. Tang and W. J. Riley

Full Screen / Esc

Printer-friendly Version

Interactive Discussion

Riley, W. J., Still, C. J., Torn, M. S., and Berry, J. A.: A mechanistic model of (H2O)-O-18 and (COO)-O-18 fluxes between ecosystems and the atmosphere: model description and sensitivity analyses, Global Biogeochem. Cy., 16, 1095, doi:10.1029/2002gb001878, 2002.

Riley, W. J., McKone, T. E., and Hubal, E. A. C.: Estimating contaminant dose for intermittent dermal contact: model development, testing, and application, Risk Anal., 24, 73–85, doi:10.1111/J.0272-4332.2004.00413.X, 2004.

Riley, W. J., Subin, Z. M., Lawrence, D. M., Swenson, S. C., Torn, M. S., Meng, L., Mahowald, N. M., and Hess, P.: Barriers to predicting changes in global terrestrial methane fluxes: analyses using CLM4Me, a methane biogeochemistry model integrated in CESM, Biogeosciences, 8, 1925–1953, doi:10.5194/bg-8-1925-2011, 2011.

Simunek, J. and Suarez, D. L.: Modeling of carbon-dioxide transport and production in soil. 1. Model development, Water Resour. Res., 29, 487–497, doi:10.1029/92wr02225, 1993.

Tang, J. Y. and Riley, W. J.: A new top boundary condition for modeling surface diffusive exchange of a generic volatile tracer: theoretical analysis and application to soil evaporation, Hydrol. Earth Syst. Sci., 17, 873–893, doi:10.5194/hess-17-873-2013, 2013.

Tang, J., Zhuang, Q., Shannon, R. D., and White, J. R.: Quantifying wetland methane emissions with process-based models of different complexities, Biogeosciences, 7, 3817–3837, doi:10.5194/bg-7-3817-2010, 2010.

Tang, J. Y., Riley, W. J., Koven, C. D., and Subin, Z. M.: CLM4-BeTR, a generic biogeochemical transport and reaction module for CLM4: model development, evaluation, and application, Geosci. Model Dev., 6, 127–140, doi:10.5194/gmd-6-127-2013, 2013.

Tans, P. P.: Oxygen isotopic equilibrium between carbon dioxide and water in soils, Tellus B, 50, 163–178, doi:10.1034/J.1600-0889.1998.T01-1-00004.X, 1998.

Venterea, R. T. and Rolston, D. E.: Mechanistic modeling of nitrite accumulation and nitrogen oxide gas emissions during nitrification, J. Environ. Qual., 29, 1741–1751, doi:10.2134/jeq2000.00472425002900060003x, 2000.

Walter, B. P. and Heimann, M.: A process-based, climate-sensitive model to derive methane emissions from natural wetlands: application to five wetland sites, sensitivity to model parameters, and climate, Global Biogeochem. Cy., 14, 745–765, doi:10.1029/1999gb001204, 2000.

Zhuang, Q., Melillo, J. M., Kicklighter, D. W., Prinn, R. G., McGuire, A. D., Steudler, P. A., Felzer, B. S., and Hu, S.: Methane fluxes between terrestrial ecosystems and the atmosphere at northern high latitudes during the past century: a retrospective analysis

Simple formulations and solutions of the dual-phase diffusive transport

J. Y. Tang and W. J. Riley

with a process-based biogeochemistry model, Global Biogeochem. Cy., 18, Gb3010, doi:10.1029/2004gb002239, 2004.

Zhuang, Q. L., Chen, M., Xu, K., Tang, J. Y., Saikawa, E., Lu, Y. Y., Melillo, J. M., Prinn, R. G., and McGuire, A. D.: Response of global soil consumption of atmospheric methane to changes in atmospheric climate and nitrogen deposition, Global Biogeochem. Cy., 27, 650–663, doi:10.1002/Gbc.20057, 2013.

Simple formulations and solutions of the dual-phase diffusive transport

J. Y. Tang and W. J. Riley

Title Page

Abstract | Introduction

Conclusions | References

Tables | Figures

◄ | ►

◄ | ►

Back | Close

Full Screen / Esc

Printer-friendly Version

Interactive Discussion

Table 1. An incomplete literature survey of different formulations that have been used for modeling dual-phase diffusive transport.

Equation	Remark	References
$\frac{\partial C_{CH_4}}{\partial t} = \frac{\partial}{\partial z}\left(D_i \frac{\partial C_{CH_4}}{\partial z}\right) + S$	Bulk soil CH_4 concentration is the primary variable. Saturated and unsaturated soil use different but constant diffusivities D_i.	Walter and Heimann (2000); Zhuang et al. (2004).
$\frac{\partial R_g C_g}{\partial t} = \frac{\partial}{\partial z}\left(D \frac{\partial C_g}{\partial z}\right) + S$	The gaseous phase is used as primary variable. The model assumes gas diffusion to dominate in unsaturated soil and aqueous diffusion to dominate in saturated soil. The water table is assumed to be at the layer interface. Diffusivity varies continuously with soil moisture.	Venterea and Rolston (2000); Riley et al. (2011)
$\frac{\partial C}{\partial t} = \frac{\partial}{\partial z}\left(D \frac{\partial C}{\partial z}\right) + S$	Bulk tracer concentration is used as the primary variable. Diffusivity varies continuously with soil moisture. Special care is put to the water–air interface.	Tang et al. (2010, 2013).
$\frac{\partial C_g}{\partial t} = \frac{\partial}{\partial z}\left(D_g \frac{\partial C_g}{\partial z}\right) + S_g$ $\frac{\partial C_w}{\partial t} = \frac{\partial}{\partial z}\left(D_w \frac{\partial C_w}{\partial z}\right) + S_w$	Tracks gaseous and aqueous phase of a given tracer separately. Gas dissolution and exsolution are considered explicitly. Diffusivity varies continuously with moisture.	Maggi et al. (2008)

Table 2. Parameters used for the steady-state CO_2 model.

Parameter	Value and Units
C_a	1.7 ppmv
D_g	$9.33 \times 10^{-6}\,m^2\,s^{-1}$
D_w	$6.667 \times 10^{-10}\,m^2\,s^{-1}$
$f_{s,1}$	0.025 m
$f_{s,2}$	0.25 for $N = 20$, 0.05 for $N = 100$
S_0	$1\,mol\,day^{-1}$
z_0	0.4 m
α	0.76
ε	$0.2\,m^3\,m^{-3}$
θ	$0.3\,m^3\,m^{-3}$

J. Y. Tang and W. J. Riley

Table 3. Parameters used for the steady-state CH_4 model.

Parameter	Value and Units
D_g	$1.267 \times 10^{-5}\,\mathrm{m^2\,s^{-1}}$
D_w	$1.33 \times 10^{-10}\,\mathrm{m^2\,s^{-1}}$
$f_{s,1}$	$0.025\,\mathrm{m}$
$f_{s,2}$	0.25 for $N = 20$, 0.05 for $N = 100$
Q_1	$10^{-6}\,\mathrm{s^{-1}}$
Q_2	$10^{-11}\,\mathrm{mol\,s^{-1}}$
z_1	$0.1\,\mathrm{m}$
z_2	$0.4\,\mathrm{m}$
α	0.0318
ε_1	$0.2\,\mathrm{m^3\,m^{-3}}$
θ_1	$0.3\,\mathrm{m^3\,m^{-3}}$
θ_2	$0.5\,\mathrm{m^3\,m^{-3}}$

J. Y. Tang and W. J. Riley

Table 4. Parameters used for the transient tracer diffusion model.

Parameter	Values and Units
C_0	$1\,\mathrm{mol\,m^{-3}}$
D_g	$5 \times 10^{-6}\,\mathrm{m^2\,s^{-1}}$
D_w	$5 \times 10^{-4}\,\mathrm{m^2\,s^{-1}}$
$f_\mathrm{s,1}$	$0.025\,\mathrm{m}$
$f_\mathrm{s,2}$	0.25 for $N = 20$, 0.05 for $N = 100$
z_1	$0.15\,\mathrm{m}$
α	0.1

Table A1. Symbols used in paper, their definitions and corresponding units.

Symbol	Definition	Units
C_a	Atmospheric tracer concentration.	$mol\,m^{-3}$
C_0	Point tracer source concentration	$mol\,m^{-3}$
C_g, C_w and C	Gaseous, aqueous and bulk tracer concentration.	$mol\,m^{-3}$
$c_{j-1/2}$	Tracer conductance between layer j and $j-1$.	$m\,s^{-1}$
D_g, D_w and D	Gaseous, aqueous and bulk diffusivity.	$m^2\,s^{-1}$
$D_{wg,j}$	Weighted tracer diffusivity in layer j.	$m^2\,s^{-1}$
$F_{w,j-1\rightarrow j}$	Aqueous tracer flux from layer $j-1$ to layer j.	$mol\,m^{-2}\,s^{-1}$
$F_{a,j-1\rightarrow j}$	Gaseous tracer flux from layer $j-1$ to layer j.	$mol\,m^{-2}\,s^{-1}$
$F_{j-1\rightarrow j}$	Bulk tracer flux from layer $j-1$ to layer j.	$mol\,m^{-2}\,s^{-1}$
$F_{g,0\rightarrow 1}$	Gaseous tracer fluxes from atmosphere into soil.	$mol\,m^{-2}\,s^{-1}$
$f_{s,1}$	Scaling parameter for numerical discretization.	m
$f_{s,2}$	Scaling parameter for numerical discretization.	None
j	Layer indices.	None
L	Column depth	m
N	Total number of numerical layers.	None
Q_1	CH_4 consumption rate.	s^{-1}
Q_2	CH_4 production rate.	$mol\,m^{-3}\,s^{-1}$
R_g and R_w	Parameters to convert gaseous and aqueous tracer concentrations into accordant bulk concentrations.	None
r_a and r_s	Atmospheric resistance and soil resistance.	$s\,m^{-1}$
S_j, $S(C_w, z)$	Net tracer source.	$mol\,m^{-3}\,s^{-1}$
S_0	Total CO_2 production rate.	$mol\,m^{-3}\,s^{-1}$
z, z_j and $z_{h,j}$	Numerical layer depths.	m
z_0	e-folding depth for soil CO_2 production.	m
z_1	Beginning of the production zone for the CH_4 model.	m
z_2	Ending of the production zone for the CH_4 model.	m
Δz_j	Numerical node thickness.	m
α	Bunsen solubility coefficient.	None
θ	Soil moisture	$m^3\,m^{-3}$
ε	Air-filled soil porosity	$m^3\,m^{-3}$

Title Page

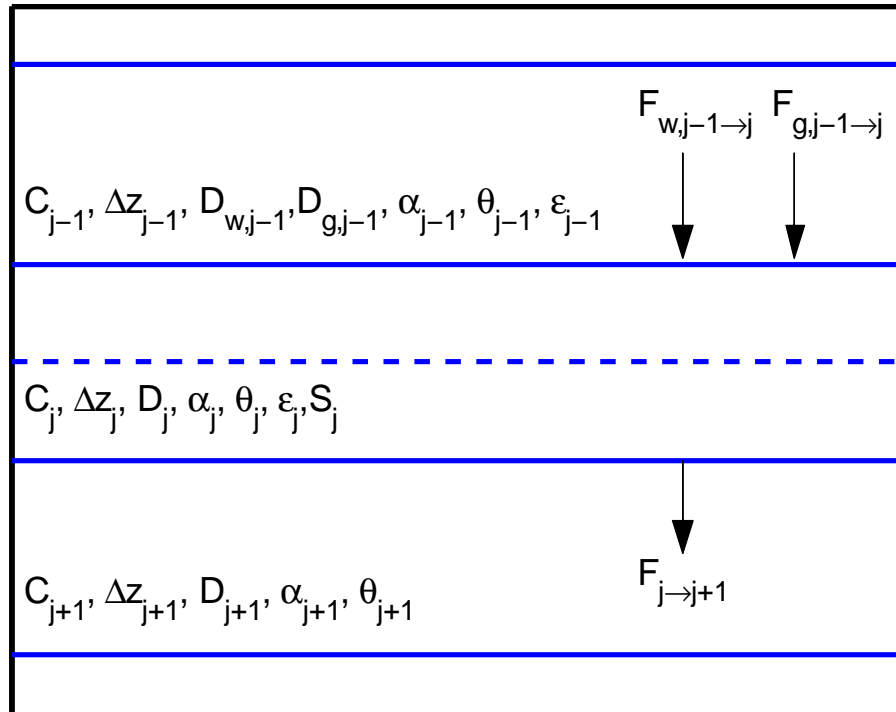Abstract | Introduction

Conclusions | References

Tables | Figures

◀ | ▶

◀ | ▶

Back | Close

Full Screen / Esc

Printer-friendly Version

Interactive Discussion

Fig. 1. Schematic of the dual-phase diffusive transport problem: solid lines are the interfaces between control volumes and the dashed line is the center of the control volume. All symbols are defined in Table A1.
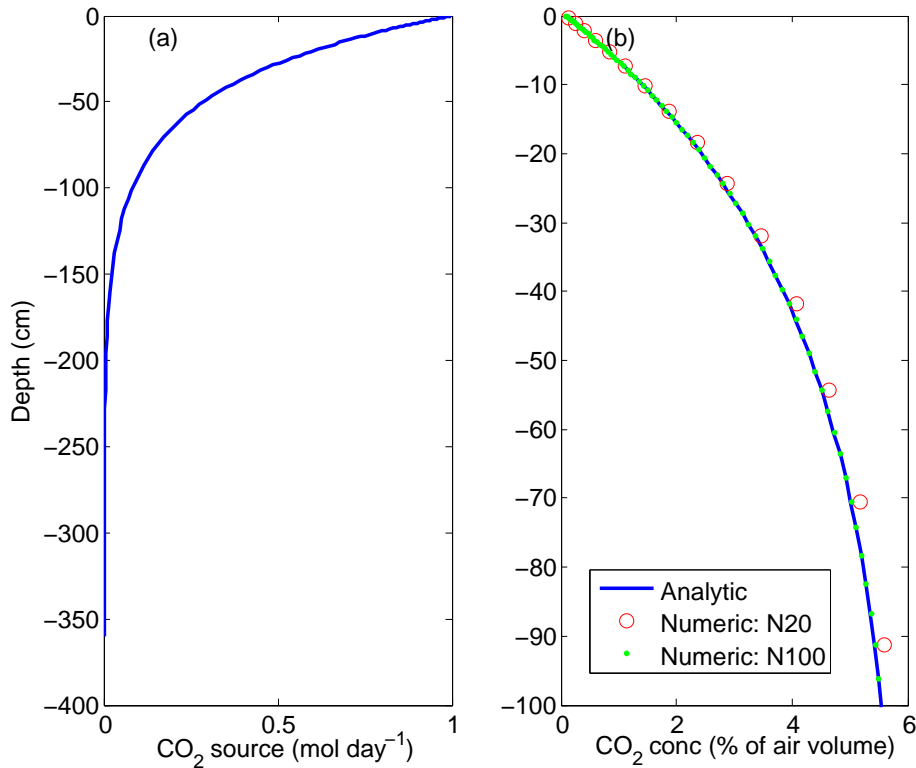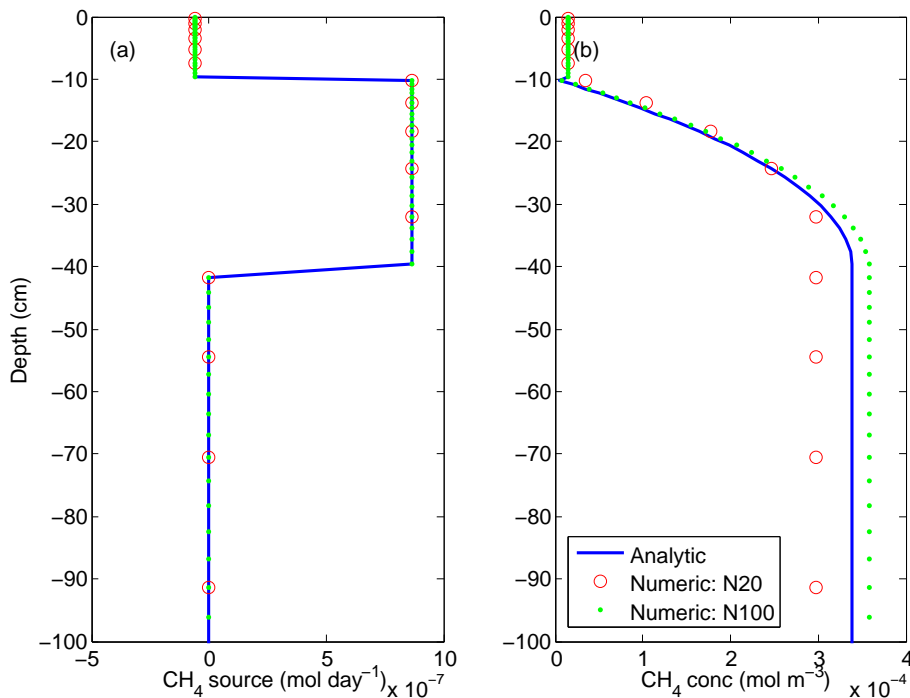
Fig. 2. Comparison between the numerical and analytical solutions for the steady-state soil CO_2 model: **(a)** net CO_2 source profile, as specified in the second term of Eq. (11); **(b)** analytical and predicted soil CO_2 profiles. N20 indicates solution using 20 numerical layers and N100 indicates solution using 100 numerical layers.

Title Page

Abstract | Introduction

Conclusions | References

Tables | Figures

◀◀ | ▶▶

◀ | ▶

Back | Close

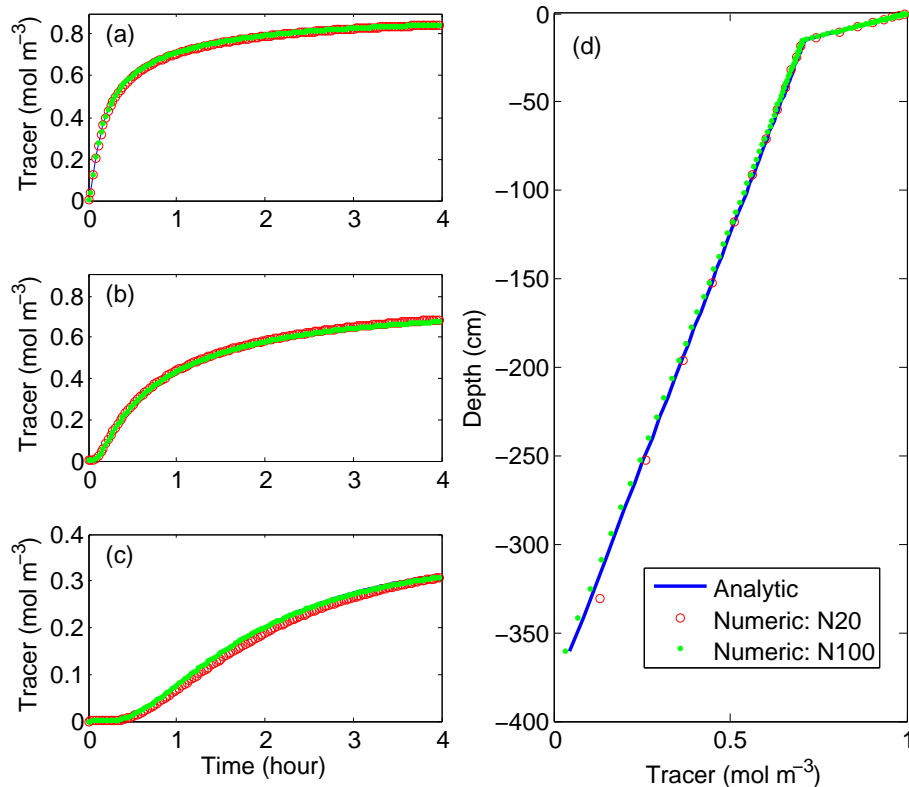Full Screen / Esc

Printer-friendly Version

Interactive Discussion

Fig. 3. Comparison between the numerical and analytical solutions for the steady-state soil methane model: **(a)** net CH_4 source profiles; **(b)** soil gaseous CH_4 profiles. N20 indicates the solution using 20 numerical layers and N100 indicates the solution using 100 numerical layers.

Fig. 4. Comparison between the numerical and analytical solutions for the point source tracer diffusion model: **(a)** temporal evolution of tracer concentration at 7 cm; **(b)** temporal evolution of tracer concentration at 15 cm; **(c)** temporal evolution of tracer concentration at 200 cm; and **(d)** steady state solution. N20 indicates the solution using 20 numerical layers and N100 indicates the solution using 100 numerical layers.